© creative

Scientific paper

# Synthesis, Characterization and Catalytic Properties of L-Cysteine-Mediated Self-Assembled Au-Ag/AgCl Nanoparticles

## Moein Rezazadeh and Zeinab Moradi-Shoeili

Department of Inorganic Chemistry, Faculty of Chemistry, University of Guilan, P.O. Box 41335-1914, Rasht, Iran

\* Corresponding author: E-mail: zmoradi@guilan.ac.ir Tel.: +98 13 33333262; fax: +98 13 33320066

Received: 02-07-2025

# **Abstract**

In this study, the self-assembly of gold and silver-based nanoclusters modified by L-cysteine (Cys@Au-Ag/AgCl) was prepared using a simple and straightforward hydrothermal method. Cys@Au-Ag/AgCl exhibited efficient catalytic activity for the rapid reduction of 4-nitrophenol (4-NP) to the less toxic 4-aminophenol (4-AP) in the presence of NaBH<sub>4</sub> as a reducing agent, completing the reaction within a few minutes with a rate constant of  $6.1 \times 10^{-3}$  s<sup>-1</sup>. The catalytic performance of Cys@Au-Ag/AgCl was optimized by studying the effect of various parameters on the catalytic reduction. In addition, Cys@Au-Ag/AgCl nanocomposite was used for catalytic reduction of K<sub>3</sub>[Fe(CN)<sub>6</sub>] in the presence of NaBH<sub>4</sub>, and the reaction rate constant was found to be  $1.73 \times 10^{-2}$  s<sup>-1</sup>. The antibacterial activity of Cys@Au-Ag/AgCl nanocomposite was also evaluated against common drug-resistant Gram-positive bacteria (*Bacillus subtilis* and *Staphylococcus aureus*) and Gram-negative bacteria (*Pseudomonas aeruginosa* and *Escherichia coli*). The results demonstrated that the multifunctional Cys@Au-Ag/AgCl nanocomposite exhibited good antibacterial activity against these clinical drug-resistant bacteria.

**Keywords:** Gold; Silver; Nanoclusters; 4-Nitrophenol; K<sub>3</sub>[Fe(CN)<sub>6</sub>]; Antibacterial activity

# 1. Introduction

Over the past decade, noble metal nanoparticles (MNPs), such as gold, silver, palladium, and platinum, have attracted considerable attention due to their unique advantages such as high strength, stability, and cost-effective production.<sup>1,2</sup> These nanoparticles exhibit multiple applications, including in electronics, photonics, catalysis, drug delivery, biological imaging, magnetic recording devices, biosensors, and as enzyme mimetic nanoparticles.<sup>3,4</sup> Bimetallic nanoparticles of noble metals usually possess advantages in comparison with their monometallic counterparts due to the synergy between the two components which allows them to exhibit a wide range of new properties and applications.<sup>5,6</sup> Structural and physico-chemical properties of bimetallic nanoparticles strongly depend on the elemental composition and the method used to produce them.<sup>7</sup> Recently, many efforts have been devoted to the construction of a ternary Au/Ag/AgCl heterostructure. Results have shown that the incorporation of AgCl in bimetallic nanostructure can provide a much higher photocatalytic perfor-

mance in comparison with pure Ag, Au and bimetallic Ag/ Au nanoparticles. Moreover, Au/Ag/AgCl hybrid materials can provide the multifunctionality of catalytic and optical properties that can be utilized in sensor and catalytic systems. Kuo et al. developed a cost-effective, highly sensitive and specific sensing system for easy and rapid detection of nanomolar concentrations of spermine in complex urine samples based on high peroxidase-like catalytic activity of Ag-Au/AgCl nanohybrid. They reported that the catalytic activity of Ag-Au/AgCl nanohybrid was at least 150-fold higher than that of its Ag, Au and AgCl components. Sapkota et al. described the facile, efficient and ecofriendly synthesis route for Au-Ag@AgCl nanomaterials possessed high catalytic activity for multicomponent tandem synthesis of various quinoline derivatives. 10 Given its excellent surface-enhanced Raman scattering (SERS), Barveen and co-workers have demonstrated a facile hydrothermal and photoreduction approach to fabricate the Ag/Au/AgCl heterostructure for the SERS detection of antibiotics and analgesics. This unique properties of Ag/Au/AgCl heterostructure in the SERS process was related to the coupling of

bimetal Au and Ag with the semiconductor (AgCl) which provides the large surface area, high enhancement of Raman signal, improvement of detection sensitivity, reproducibility and uniformity and also the reusable properties of SERS substrate due to the photodegradation ability of Ag-Cl.<sup>11</sup> Devi et al. reported the catalytic and antimicrobial properties of Ag/Au/AgCl nanoparticles fabricated by using Aquilaria agallocha leaf juice. They found that the Au@Ag@ AgCl nanoparticles showed better antimicrobial properties than the monometallic Ag and Au nanoparticles because of the medicinal properties of the leaf. The as-prepared Ag/ Au/AgCl nanoparticles demonstrated an excellent catalytic activity in the reduction of toxic nitrocompounds.12 Recently, Au@Ag@AgCl nanoparticles were employed for visible-light-driven photocatalytic degradation of various organic pollutants by Ryu and and co-workers.<sup>13</sup> In another precedent on photocatalytic activity of Ag/Au/AgCl hybrid materials, Lio et al. fabricated one-dimensional (1D) Ag/ Au/AgCl hollow heterostructures. It was found that the synthesized Ag/Au/AgCl hollow heterostructures showed the higher catalytic and photocatalytic activity as compared to pure Ag nanowires. However, the AgCl semiconductor could act as supporting materials, but the excess AgCl is the obstacle for contact of Ag/Au bimetals with reactive species. Moreover, they showed that the Ag/Au bimetals enhanced the photocatalytic performance of AgCl semiconductor via the localized surface plasmon resonance (LSPR) and plasmon resonance energy transfer (PRET) mechanisms.<sup>14</sup>

4-Nitrophenol (4-NP) is highly toxic pollutant which can cause several negative impacts on human health such as formation of methemoglobin, liver and kidney damage, anemia, skin irritation, eye irritation, and systemic poisoning. 15 This pollutant has been listed as a priority pollutant by the US Environmental Protection Agency. Over the years, various methods such as photocatalytic degradation, chemical oxidation, electrochemical treatments, adsorption and coagulation have been developed to minimize the pollution of nitrophenols from wastewater. 16 In recent years, chemically reduction of nitrophenols to the useful product aminophenols using sodium borohydride (NaBH<sub>4</sub>) as a reducing agent has been commonly used as the effective removal methodology for such hazardous substrate compounds from polluted waters. 17,18 In addition, there is a high industrial demand for aromatic amine compounds.<sup>19</sup> As an example, in pharmaceutical industry, the conversion of nitrophenols to aminophenols can be widely used in the production of many analgesics and antipyretics such as paracetamol and phenacetin. <sup>20,21</sup> These reactions have been also utilized as model reaction to assess the catalytic performance of various nanocatalytic systems especially metallic nanoparticles. 17,22 This is because the progress of the reduction reaction can be easily followed by UV-vis spectroscopy during the conversion of nitrophenols to aminophenols. Up to now, there have been a large number of mono and bimetallic nanoparticles consisting of Au and Ag have been reported for the catalytic

reduction of nitroaromatic compounds.<sup>23-28</sup> However, the combination of Au, Au and AgCl nanoparticles is rarely investigated.

The World Health Organization (WHO) reported that antimicrobial resistance is one of the top 10 health threats to humans in recent years. According to the WHO report, bacterial infection has been one of the main causes of death worldwide in the past 15 years.<sup>29</sup> Although antibiotics have achieved remarkable success as conventional antibacterial drugs in the treatment of bacterial infections, the widespread and inappropriate use of antibiotics leads to antimicrobial resistance.<sup>30</sup> MNPs have been found as effective mineral agents in presenting antibacterial properties and optimizing their antibacterial performance is a major area of interest in new antibacterial treatments. 31,32 The chemical and physical nature of MNPs such as their elemental composition and morphology can significantly contribute to the interactions between MNPs and the target biosystem enhancing the development of more efficient antibacterial agents. 33-35

Herein, novel L-cysteine-modified Au and Ag/AgCl nanoclusters (Cys@Au-Ag/AgCl) were developed via a simple hydrothermal method. This work advances prior research on mono/bimetallic Au/Ag nanoparticles by introducing a ternary system with unique synergistic properties. The Cys@Au-Ag/AgCl nanocomposite demonstrates enhanced catalytic efficiency for reducing both organic (4-NP) and inorganic (K<sub>3</sub>[Fe(CN)<sub>6</sub>]) pollutants to less toxic products, along with potent antibacterial activity against clinical drug-resistant Gram-positive and Gram-negative bacteria. These dual capabilities make the Cys@Au-Ag/AgCl nanocomposite a promising candidate for environmental and biomedical applications.

# 2. Experimental

#### 2. 1. Materials and Characterization

All the chemicals used in this study were obtained from either Sigma-Aldrich or Merck and used as received without further purification. Deionized water was used throughout all the experiments.

Scanning electron microscopy (SEM) images were obtained using a field-emission scanning electron microscope (FE-SEM, TESCAN MIRA3, TESCAN Co., Czech Republic) at an acceleration voltage of 3 KV. UV-vis spectroscopic measurements were performed using a UV-vis spectrophotometer) Shimadzu UV-1800, Japan). FTIR spectra were recorded on an FTIR spectrophotometer (Alpha-Bruker) using KBr disks at room temperature. X-ray diffraction (XRD) spectroscopy was performed using an X-ray diffractometer (Philips PW 1730, Netherlands) with Cu K $\alpha$  radiation ( $\lambda$  = 1.54 Å, 40 kV × 30 mA), and 2 $\theta$  was scanned from 10° to 80°. X-ray energy diffraction (EDAX) was performed using an X-ray energy diffractometer (EM8000F, KY KY CO.,China).

# 2. 2. Synthesis of L-Cysteine Modified Cys@ Au-Ag/AgCl Nanocomposite

Self-assembled gold-silver nanoparticles with L-cysteine were prepared by a facile hydrothermal reduction method using l-cysteine as reducing and stabilizing agent. In this method, 1ml of HAuCl<sub>4</sub> solution (0.01M) and 1 ml of AgNO<sub>3</sub> solution (0.01M) were added to 10 mL deionized water. Then, 2 ml of l-cysteine solution (0.1M) was added dropwise under vigorous stirring for 10 minutes at room temperature. The pH of the solution was adjusted to 12 using NaOH (0.1M). A dark-brown colloidal precipitate was obtained, which was kept in autoclave at 120 °C for 2 hours. Then final precipitate was separated by centrifugation, washed three times with water and once with ethanol and dried at room temperature and washed three times with water and once with ethanol and dried at room temperature.

# 2. 3. Reduction of 4-Nitrophenol to 4-Aminophenol

To assess the catalytic performance of Cys@Au-Ag/AgCl nanocomposite, the reduction of 4-NP to 4-AP was used as a model reaction. In a typical experiment, 300 μl solution of freshly prepared aqueous NaBH<sub>4</sub> (0.1M) was added to 2.5 ml aqueous solution of 4-NP (0.1 mM) in a quartz cuvette with 1.0 cm path length. The color of the solution changed immediately from pale to bright yellow upon the addition of NaBH<sub>4</sub>. Then, 5 mg of the synthesized Cys@Au-Ag/AgCl nanocomposite was added to the reaction mixture and the initial yellow color of the solution faded to colorless as the reaction proceeded. The progress of the reduction reaction was followed by monitoring the absorbance of the solution over the wavelength range of 250–500 nm in the same time interval.

The reduction percentage of 4-NP to 4-AP was calculated using eq. (1):

%Reduction of 
$$4 - NP = \frac{A_0 - A_t}{A_0} \times 100\%$$
 (1)

where  $A_0$  is initial absorbance and  $A_t$  the absorbance after a time interval.

# 2. 4. Investigation of the Effect of Different Parameters on the Catalytic Activity

In order to investigate the effect of catalyst dispersion on reaction rate, 0.01 g of the synthesized nanocomposite was dispersed in 10 mL of water and sonicated for 15 minutes. Then, Cys@Au-Ag/AgCl aqueous dispersion (1 mg/mL, 500  $\mu L$ ) was added to the aqueous solutions of 4-NP (0.1 mM, 2.5 mL) and NaBH $_4$  (0.1M, 300  $\mu L$ ) and the absorbance of the reaction solution was analyzed at 250-500 nm during the time course.

To optimize the amount of catalyst, reduction reac-

tion of 4-NP was repeated four times under the same concentration of 4-NP (0.1 mM, 2.5 mL) and NaBH<sub>4</sub> (0.1M, 300  $\mu L)$ , except that different amount of the catalyst was added (200, 500 and 700  $\mu L$ , 1 mg/mL) to the reaction mixture.

The effect of concentration of NaBH<sub>4</sub> on the rate of the catalytic reducing of 4-NP was also studied. In this regards, different amount of NaBH<sub>4</sub> (200, 300, 400 and 700  $\mu$ L, 0.1 M) were added to the 4-NP solution (0.1 mM, 2.5 mL) and Cys Au/Ag nanocomposite (1 mg/mL, 500  $\mu$ L).

To investigate the effect of the complex water environment on the catalytic performance of Cys@Au-Ag/Ag-Cl nanocomposite in the reduction of 4-NP, the same molar concentration of 4-NP solutions were also prepared in tap water and seawater instead of the deionized water and the absorbance of the reaction solution was analyzed at 250-500 nm during the time course. The tap water directly obtained from the laboratory (without any treatment) and the Caspian seawater were used instead of deionized water when preparing the 4-NP solution.

## 2. 5. Reduction of $K_3[Fe(CN)_6]$

The catalytic activity of Cys@Au-Ag/AgCl nanocomposite was also studied in the reduction of  $K_3$  [Fe(CN)6]. In a typical experiment, freshly prepared aqueous NaBH4 solution (0.1 M, 200  $\mu L$ ) was mixed with aqueous solution of  $K_3$  [Fe(CN)6] (0.2 mM, 2.5 mL) in a quartz cuvette and then the Cys@Au-Ag/AgCl aqueous suspension (500  $\mu L$ , 1 mg/mL) was injected without any stirring. The reaction was monitored by taking the absorption spectra between 250–500 nm at a time interval of 1 minutes. The reduction percentage of  $K_3$  [Fe(CN)6] was calculated using eq. (2):

%reduction of 
$$K_3 Fe(CN)_6 = \frac{A_0 - A_t}{A_0} \times 100 \%$$
 (2)

where  $A_0$  is initial absorbance and  $A_t$  the absorbance after a time interval at  $\lambda = 400$  nm.

# 2. 6. Antibacterial Activity Assessment Method

The in vitro antibacterial activity of the prepared Cys@Au-Ag/AgCl nanocomposite was tested using the zone inhibition method,  $^{37}$  against four pathogenic bacteria including *Pseudomonas aeruginosa* (*P. aeruginosa*), *Escherichia coli* (*E. coli*), *Staphylococcus aureus* (*S. aureus*), and *Bacillus subtilis* (*B. subtilis*). The nutrient agar and nutrient broth cultures were prepared according to manufactures' instructions and were incubated at 37 °C. After incubation for the appropriate time, a suspension of  $100 \mu L$  of each bacterial test organism was spread onto the nutrient agar plates. Agar wells were prepared with the help of a sterilized glass tube. Then  $100\mu L$  of the test agents at a concentration of  $1000 \mu g/mL$  in DMSO were added to each well. All the bacterial strains were incubated at 37 °C for 24

h. Clear zones around the wells showed inhibition of bacterial growth and turbidity indicated bacterial resistance to the compound at the concentration present in the medium. The diameter of inhibition zones was determined in millimeters (mm). The concentration of DMSO in the medium did not affect growth of any of the microorganisms tested. Antibacterial activity of Cys@Au-Ag/AgCl nanocomposite was compared with tetracycline as standard drugs. DMSO was used as a negative control.

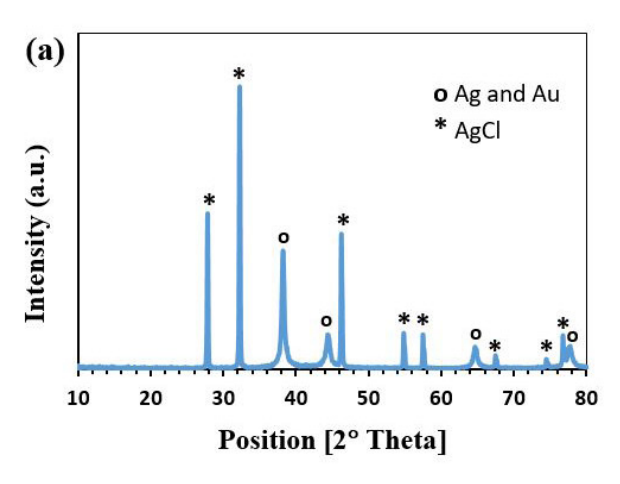
## 3. Results and Discussion

#### 3. 1. Characterization

XRD analysis was carried out to confirm the crystal structure and particle size of the synthesized nanocomposite within the range of  $2\theta = 10^{\circ}-80^{\circ}$ . It clearly shows that the sample is composed of metallic Ag/Au and cubic AgCl crystals. Ag and Au crystals cannot be distinguished in the XRD patterns because the XRD diffraction peak pattern of single metallic gold and silver NPs as well as their bimetallic NPs are close together and they have similar crystal structure and lattice constants.<sup>25</sup> As shown in Fig. 1a, the XRD pattern of the Cys@Au-Ag/AgCl nanocomposite showed four diffraction peaks at  $2\theta$ = 38.27°, 44.42°, 64.58°, and 77.72° (labeled as circles) correspond to (111), (200), (220), and (311) lattice planes of fcc structure for Au and Ag in this bimetallic system. 38,39 In addition, the XRD pattern of the nanocomposite showed diffraction peaks at  $2\theta$  = 27.88°, 32.28°, 46.28°, 54.82°, 57.47°, 67.48°, 74.47 and 77.72° (labeled as stars) were can be attributed to the (111), (200), (220), (311), (222), (400), (331) and (420) planes of the cubic crystals of AgCl. 40 Therefore, the XRD result confirms the successful formation of Cys@Au-Ag/AgCl nanocomposite. FTIR spectroscopic measurement was used to identify the binding of the L-Cysteine as capping molecules on the surface of Cys@Au-Ag/AgCl nanocomposite. Fig. 1b shows the FTIR spectra of pure L-Cysteine and Cys@ Au-Ag/AgCl. In the spectrum of pure L-Cysteine, characteristic bands of O-H stretching (3424 cm<sup>-1</sup>) and CH<sub>2</sub> stretching (2968 cm<sup>-1</sup>) were observed. 41 The broad absorption at around 3200 cm<sup>-1</sup> can be attributed to the stretching mode of ammonium. The bands at 1544 cm<sup>-1</sup> and 1593 cm<sup>-1</sup> was ascribed to the symmetric bending mode of the N-H and COO asymmetric mode, respectively.<sup>42</sup> In the case of Cys@Au-Ag/AgCl nanocomposite, several peaks of L-cysteine are seen, indicating the incorporation of the L-cysteine into the structure of final nanocomposite. In addition, comparing with the two spectra shows the decrease in intensity or shifting of some bands which indicates the interaction of L-Cysteine with the Au, Ag and AgCl nanoparticles in the prepared nanocomposite. The FTIR spectrum of L-cysteine exhibits a typical S-H vibrational band at 2553 cm<sup>-1</sup> which is absent in FTIR spectrum of Cys@ Au-Ag/AgCl, indicating that the sulfur-hydrogen bond was broken and the L-cysteine molecules were associated with Au-Ag/AgCl nanoparticles through the formation of Au/Ag-sulfur bond. Binding of L-cysteine on the surface of nanoparticles through a thiolate linkage has already been reported in the literature.<sup>43</sup>

The morphology and particle size distribution of the as-prepared Cys@Au-Ag/AgCl nanocomposite were characterized by scanning electron microscopy (SEM). As shown in Fig. 2 at different magnifications, the nanocomposite exhibits a crystalline structure composed of spherical nanoparticles with diameters predominantly below 100 nm. While most particles self-assemble into larger spherical aggregates (<500 nm), isolated nanoparticles (~20 nm) are also observed. This agglomeration behavior, commonly observed in metal nanocomposites, can be attributed to the high surface energy of these particles due to their nano-size regime. 44 The SEM analysis confirms the successful formation of a nanostructured composite with the expected morphological features.

EDX and EDS spectroscopy was performed to determine the elemental composition of Cys@Au-Ag/AgCl nanocomposite. Fig. 3a shows the EDX spectrum, which displays the peaks corresponding to Au, Ag and Cl elements,



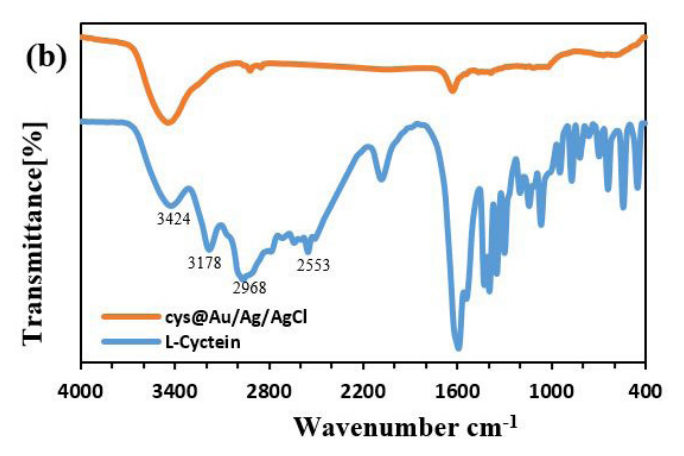


Fig. 1. (a) XRD pattern of Cys@Au-Ag/AgCl and (b) FTIR spectra of Cys@Au-Ag/AgCl and L-Cyctein

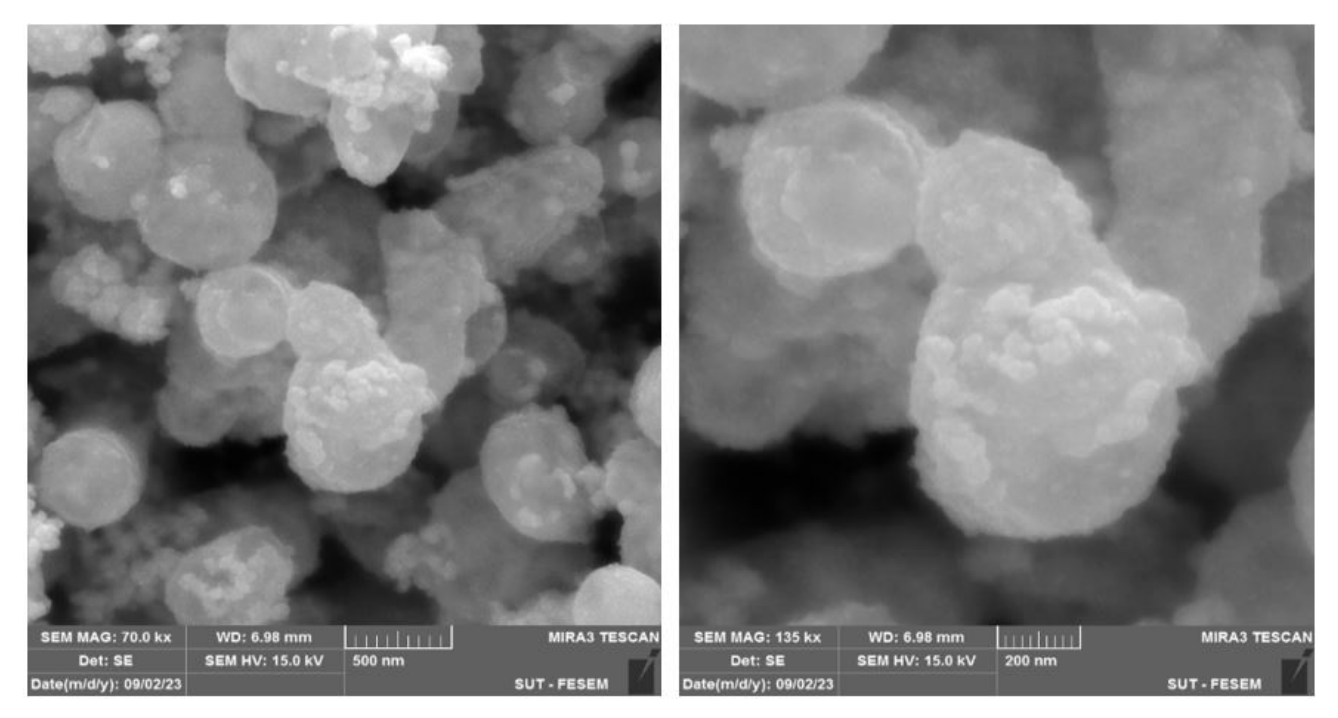


Fig. 2. SEM images of Cys@Au-Ag/AgCl nanocomposite at different magnifications (70 kx and 135 kx).

confirms the formation of Au, and Ag/AgCl NPs. The remaining elements (C, O, N and S,) due to the presence of cysteine molecules confirm the formation of Cys@Au-Ag/AgCl nanocomposite. EDS mapping of the synthesized nanocomposite (Fig. 3b) shows that all these elements are well dispersed in the structure of Cys@Au-Ag/AgCl nanocomposite.

# 3. 2. Catalytic Performance of Cys@Au-Ag/ AgCl Nanocomposite

# 3. 2. 1. Catalytic Activity of Cys@Au-Ag/AgCl in the Reduction of 4-NP

The reduction of 4-NP to 4-AP was investigated as a model reaction to study the catalytic activity of Cys@Au-Ag/AgCl nanocomposite in the presence of NaBH<sub>4</sub> (scheme 1). In the absence of catalyst, the reduction of 4-NP was negligible whereas the addition of 5 mg Cys@ Au-Ag/AgCl to 2.5 mL of the reaction mixture achieved a reduction of about 84% within 20 minutes (no stirring or sonication applied). Time-dependent UV-vis absorption spectra were recorded to monitor the reaction progress. Upon adding NaBH<sub>4</sub> to the 4-NP solution, the absorption peak shifted from 317 nm to 400 nm, accompanied by a color change from light yellow to bright yellow (Fig. 4a). This shift corresponds to the formation of 4-nitrophenolate ion (4-NP<sup>-</sup>) in alkaline conditions. In the absence of the catalyst, this peak remained the same even after a long time without a change in intensity which indicates that NaBH<sub>4</sub> alone is not able to proceed fast enough the reduction reaction. In the presence of the Cys@Au-Ag/AgCl nanocomposite, the peak at 400 nm gradually decreased while a new peak appeared at about ~300 nm, indicative of 4-AP formation. After about 20 minutes, the complete disappearance of the 400 nm peak and the decolorization of the solution mixture confirmed the successful reduction of 4-NP to 4-AP (Fig. 4b).

**Scheme 1.** Reduction of 4-NP to 4-AP in the presence of Cys@Au-Ag/AgCl nanocomposite

The catalytic activity of the prepared Cys@Au-Ag/AgCl nanocomposite in reduction of 4-NP was studied under different conditions including the effect of catalyst dispersion and different molar equivalents of catalyst and NaBH4. In order to investigate the effect of catalyst dispersion on the reaction rate, the 10 mg of Cys@Au-Ag/AgCl was dispersed in 10 mL of H2O using ultrasonication and appropriate amount was added to the reaction mixture. The results indicated that dispersing the catalyst in the reaction medium significantly increased the reaction rate as shown on Fig. 5a which provides the conversion of about 93% from 4-NP to 4-AP. The post-reaction analyses were similarly conducted under sonication to ensure sample

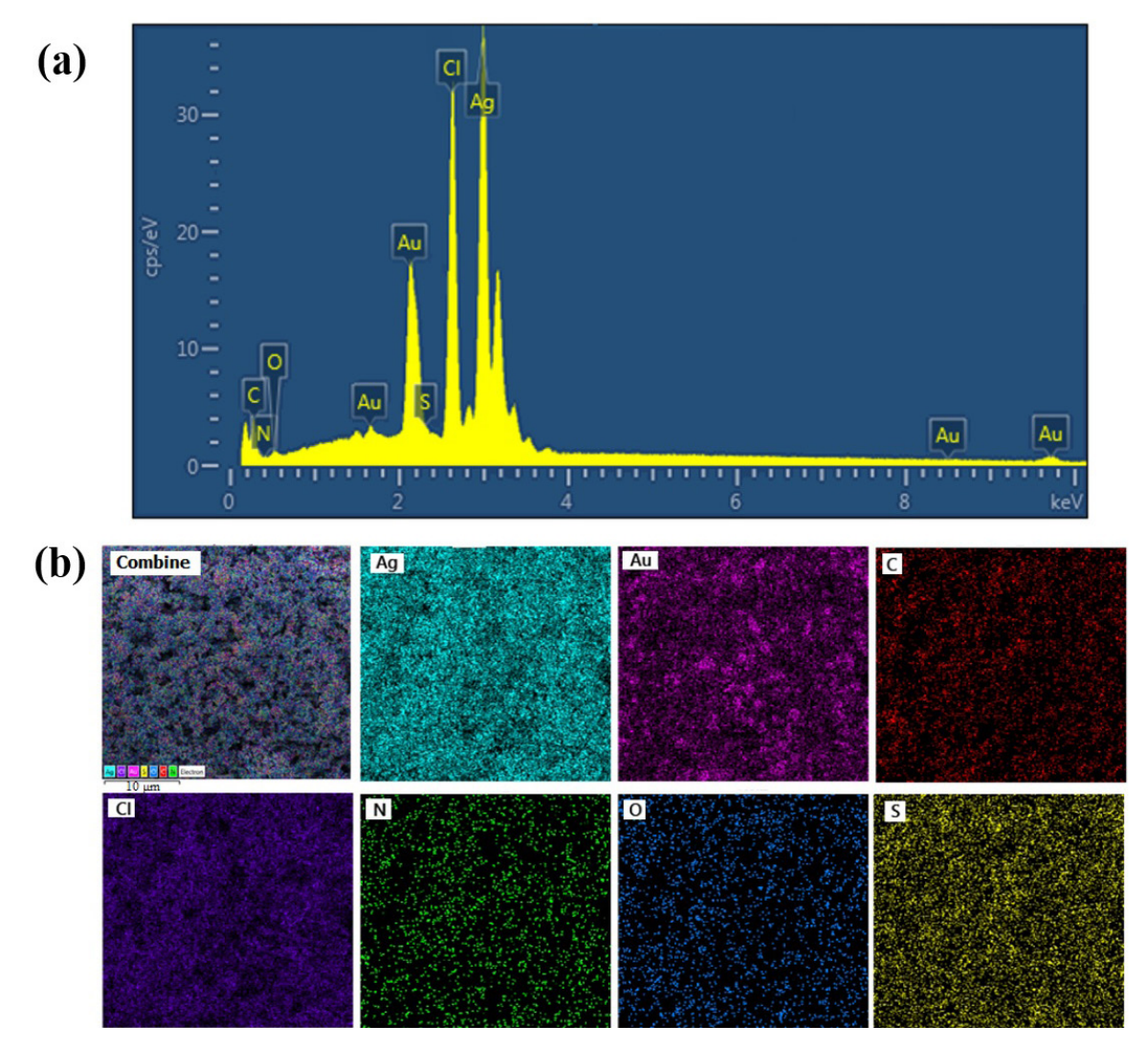


Fig. 3. (a) EDX spectrum and (b) EDS elemental mapping of the Cys@Au-Ag/AgCl nanocomposite

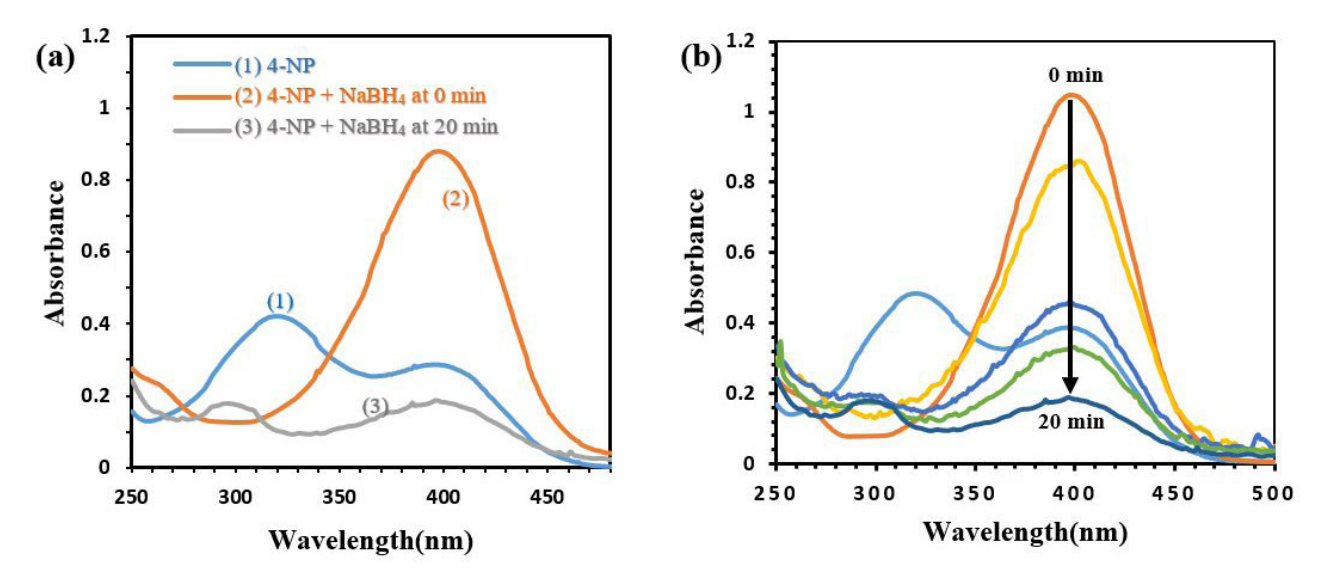


Fig. 4. (a) UV-Vis spectral profile of 4-NP and (b) Successive UV-vis absorption spectra for the reduction of 4-NP in the presence of Cys@Au-Ag/AgCl over time.

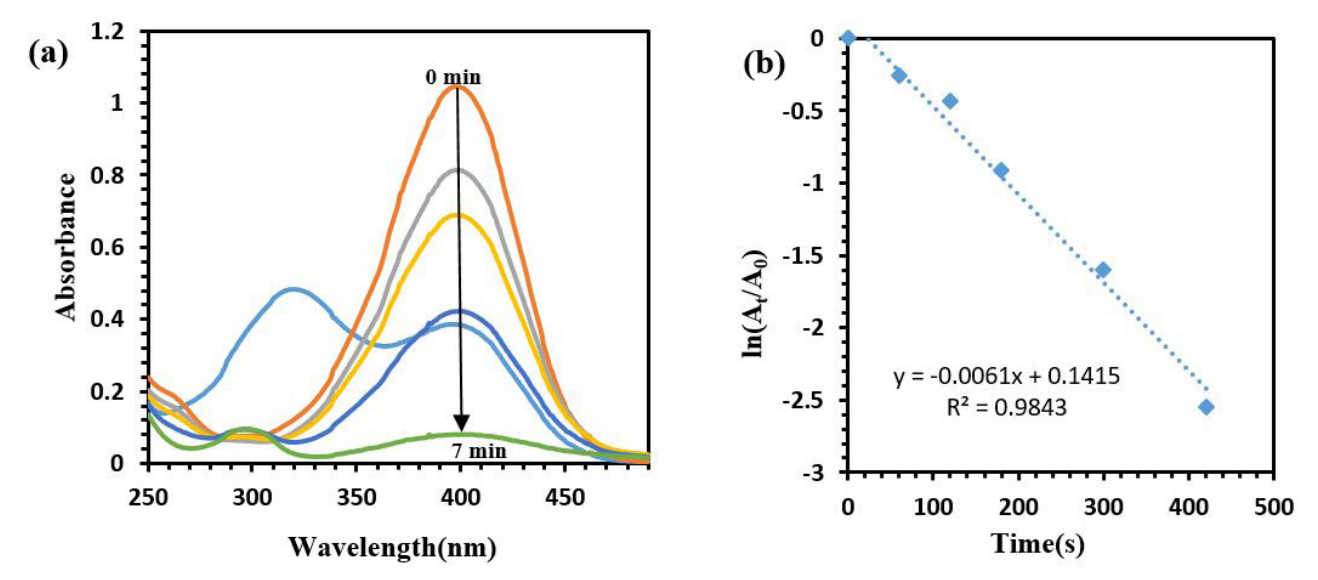


Fig. 5. (a) Sequential UV-vis absorption spectra for the sonication-assisted reduction of 4-NP by NaBH<sub>4</sub> in the presence of Cys@Au-Ag/AgCl. (b) The fitting plot curve of  $\ln(A_t/A_0)$  versus time for the catalytic reduction reaction.

uniformity. The reaction rate for the sonication-assisted reduction reaction was determined by plotting the graph of  $\ln (A_t/A_0)$  over time, where  $A_0$  and  $A_t$  are the absorbances at 400 nm at time t=0 and time t (Fig. 5b). A linear relation with a correlation coefficient of 0.9843 was obtained indicating a pseudo-first-order kinetics and the rate constant ( $k_{app}$ ) was found to be  $6.1 \times 10^{-3}$  s<sup>-1</sup>.

The optimization of the catalyst amount was achieved by varying the amount of Cys@Au-Ag/AgCl nanocomposite and the other reaction parameters during the mentioned reaction were kept constant. All optimization experiments were evaluated after a consistent 7-minute reaction period to enable direct comparison. As shown in Fig. 6a, the 0.2 mg/mL catalyst concentration achieved 93% conversion within 7 minutes, while increasing the amount to 0.28 mg/mL only marginally im-

proved the conversion to 95%. Therefore, 0.2 mg/mL concentration was selected as optimal due to its near-identical catalytic efficiency coupled with significantly lower material consumption. In order to investigate the effects of the NaBH<sub>4</sub> concentration on the reaction rate, different amounts of NaBH4 were added to the reaction vessel and the concentration of 4-NP and Cys@ Au-Ag/AgCl (0.2 mg/mL) were kept constant. According to the Fig. 6b, the highest conversion percentage (96%) was achieved at a NaBH₄ concentration of 0.012 M after 7 minutes of reaction time, while other concentrations showed progressively reduced efficiency. This optimal concentration was therefore selected for the further studies. R Madhushree et al. have also found comparable optimized conditions for 4-NP reduction using MoS<sub>2</sub>/ZnO nanocomposite.45

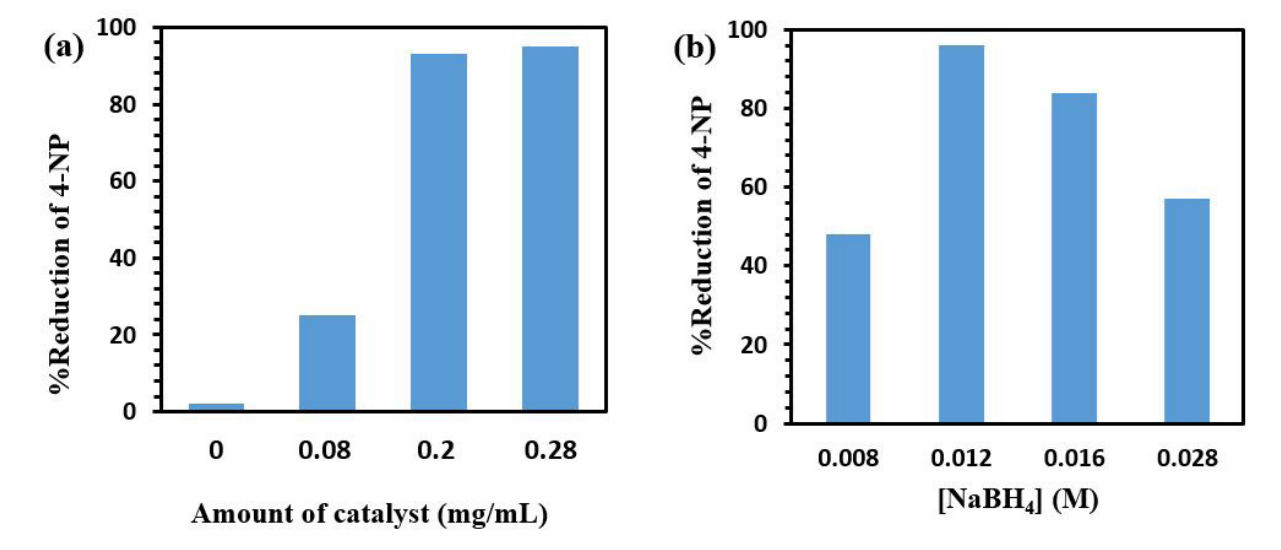


Fig. 6. Conversion of 4-NP to 4-AP in the presence of different (a) catalyst amounts (b) NaBH<sub>4</sub> concentrations after 7 minutes reaction time.

Table 1. Comparison of the catalytic performance of Cys@Au-Ag/AgCl with different nano-catalysts for 4-NP reduction.

Catalyst	Reaction conditions (4–NP, NaBH <sub>4</sub> , catalyst)	$k_{app}$ (s <sup>-1</sup> )	%Reduction, Time	Ref.
MoS <sub>2</sub> /ZnO	0.5 mM (100 mL), 500 mg, 0.1 g	$0.81 \times 10^{-3}$	99%, 15 min	45
Fe <sub>2</sub> O <sub>3</sub> -Pt@DSL-Pt	0.1mM, 50 mM, 0.5 mg	$6.32 \times 10^{-3}$	99%, 8 min	46
PtNPs@C-PZS	0.1mM, 5mM,0.2 mg	$4.6 \times 10^{-3}$	87.6%, 16 min	47
PZS@Ag-Au	0.05 mM, 3.8 mM,0.05 mg	$4.63 \times 10^{-3}$	99%, 8 min	48
Ag-Fe <sub>3</sub> O <sub>4</sub> @chitin	0.1 mM, 0.1 M, 0.075 mg	$5.23 \times 10^{-3}$	99%, 10 min	49
CoMn <sub>2</sub> O <sub>4</sub> /APTPOSS@FPS	0.2 mM, 0.5M, 0.4 mg	$1.83 \times 10^{-2}$	99%, 100 s	50
Cys@Au-Ag/AgCl	0.1 mM , 0.012 M, 0.5 mg	$6.1\times10^{-3}$	96%, 7 min	This work

As evidenced by the data in Table 1, the synthesized Cys@Au-Ag/AgCl catalyst demonstrates superior performance to previously reported nanocatalysts in terms of rate constant (k) and reaction completion time.

The catalytic performance of Cys@Au-Ag/AgCl was also investigated in different water environments such as

seawater system and tap water system instead of deionized water. As shown in Fig. 7, the synthesized nanocomposite exhibited good catalytic activity in both seawater and drinking water and the presence of interfering ions such as sulfate and carbonate salts or organic species in the water environment did not interfere significantly in 4-NP reduc-

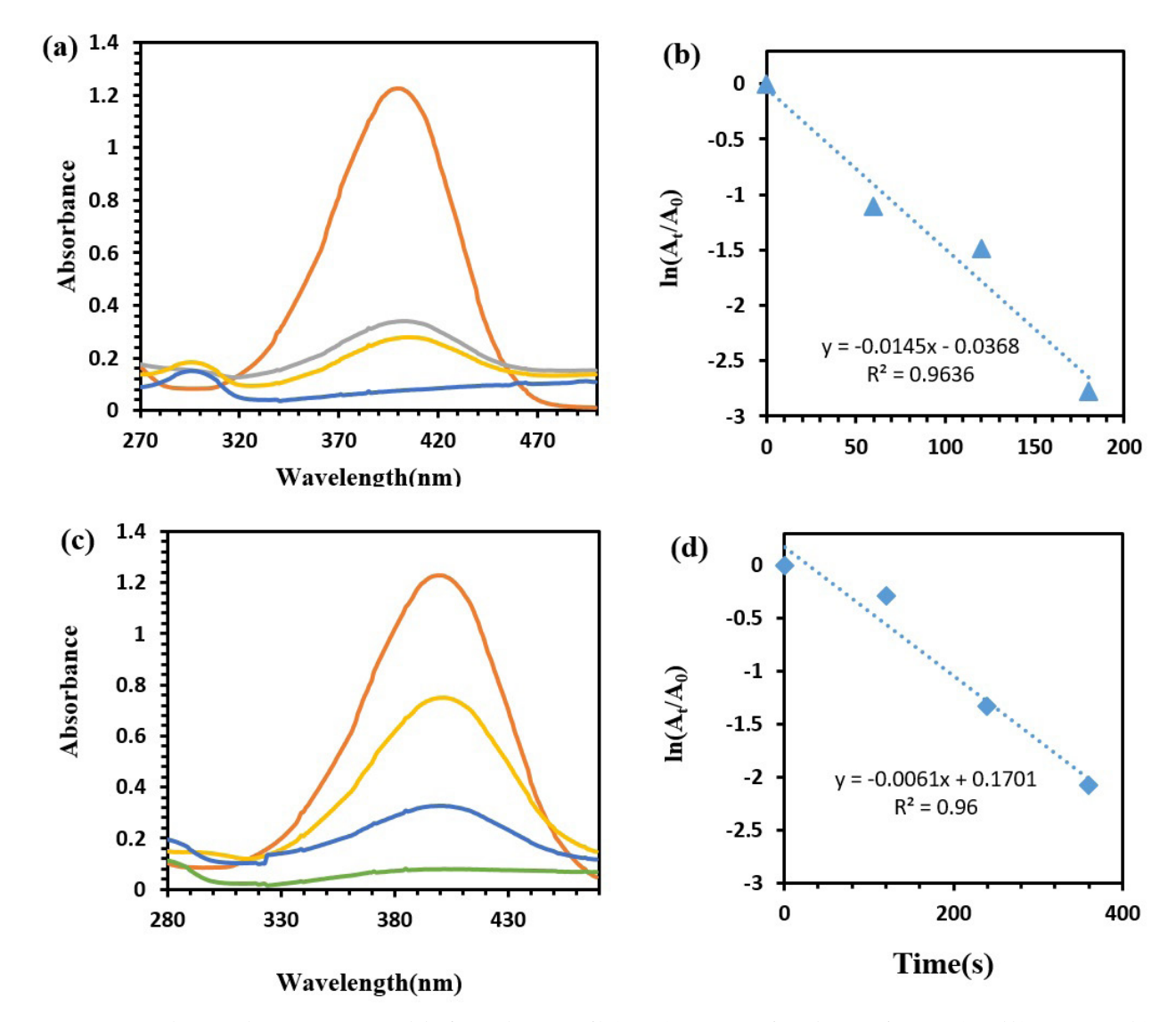
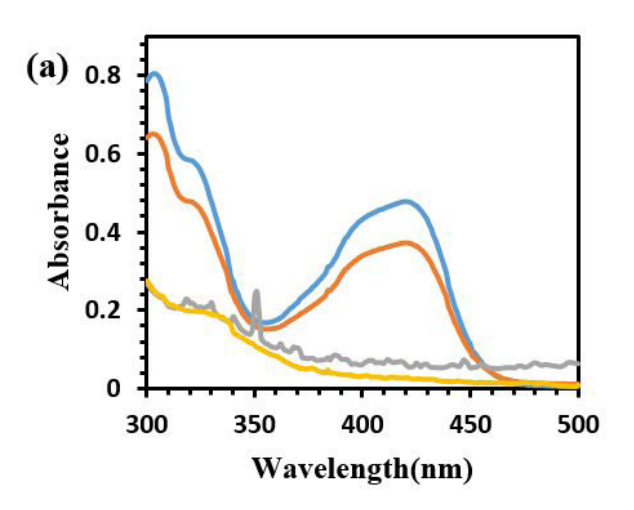


Fig. 7. Sequential UV-vis absorption spectra and the fitting plot curve of ln(At/A0) versus time for reduction of 4-NP in (a and b) tap water and (c and d) seawater in the presence of Cys@Au-Ag/AgCl nanocomposite.

tion process. The conversion efficiency of all three systems exceeds 95%.

# 3. 2. 2. Catalytic Activity of Cys@Au-Ag/AgCl in the Reduction of K<sub>3</sub>[Fe(CN)<sub>6</sub>]

The catalytic activity of Cys@Au-Ag/AgCl nano-composite was also evaluated in reduction of  $K_3[Fe(CN)_6]$  to  $K_4[Fe(CN)_6]$  in the presence of NaBH<sub>4</sub> (Fig. 8a). As shown in Fig. 8b, from  $\ln(A_t/A_0)$  vs. time plot, Cys@Au-Ag/AgCl shows pseudo-first-order kinetics reaction in reduction of  $K_3[Fe(CN)_6]$  with  $k_{app}$  value of  $1.73 \times 10^{-2} \, \mathrm{s}^{-1}$  and the conversion of 96% was achieved during 3 minutes (Fig 8b).



presence of gold and silver in the structure and their interactions with bacterial cells. Noble metal nanoparticles, particularly Ag and Au, are well-known for their bactericidal properties<sup>51</sup>. Research indicates that Ag- and Aubased nanomaterials exert antimicrobial effects through multiple pathways, including electrostatic adhesion to negatively charged bacterial membranes, penetration into cells due to their nanoscale size<sup>52</sup>, and subsequent disruption of vital cellular processes. In addition, these nanoparticles induce oxidative stress via reactive oxygen species (ROS) generation, interfere with DNA/RNA replication, and disrupt enzymatic activity by binding to essential metabolites<sup>53</sup>. Notably, Au is less reactive than Ag in oxygen-rich environments, leading to lower ROS produc-

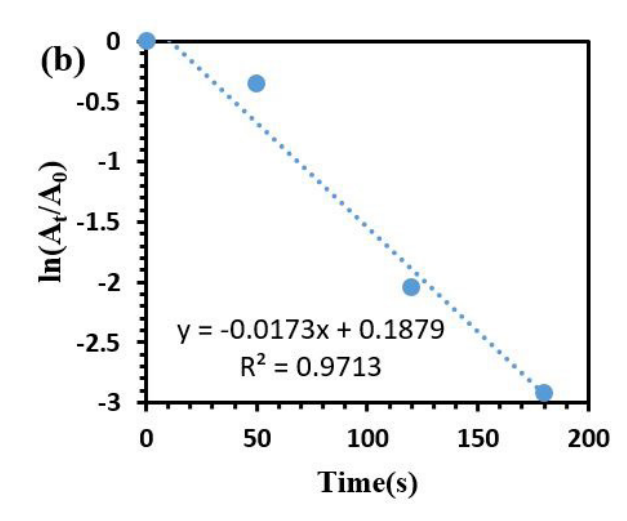


Fig. 8. (a) UV-vis spectra of the reduction of  $K_3[Fe(CN)_6]$  pollutant in the presence of Cys@Au-Ag/AgCl nanocomposite. (b) The fitting plot curve of  $ln(A_t/A_0)$  versus time for the catalytic reduction reaction.

# 3. 3. Cys@Au-Ag/AgCl Antibacterial Test on Gram-positive and Gram-negative Bacteria

The antibacterial activity of Cys@Au-Ag/AgCl nanocomposite was studied against Gram-positive bacteria, B. subtilis and S. aureus, and also Gram-negative bacteria, P. aeruginosa and E. coli, using the zone inhibition method. Tetracycline was used as positive controls. The antibacterial activity was monitored at a concentration of 1000 µg/mL in DMSO and the experiments were performed by measuring the inhibition zone around the well. The results showed that the Cys@Au-Ag/AgCl nanocomposite has significant antibacterial activity against Gram-negative bacteria compared to Gram-positive bacteria. The inhibition zone was about 15 mm for E. coli and 18 mm for P. aeruginosa. While B. subtilis showed resistance and no inhibition halo was observed, the inhibition zone for S. aureus was 18 mm. The probable antibacterial mechanism of Cys@Au-Ag/AgCl nanocomposite can be attributed to the

tion<sup>54</sup>. However, studies indicate that Ag–Au nanocomposites often exhibit superior antimicrobial activity compared to their monometallic counterparts, likely due to synergistic effects<sup>55</sup>. Therefore, Cys@Au-Ag/AgCl nanocomposite can be used as an antibacterial agent in various industries such as pharmaceuticals, food, and medicine.

#### 3. 4. Conclusion

In this study, L-cysteine was used as a biocompatible and stabilizing reducing agent to electrostatically immobilize Au, Ag and AgCl nanoparticles. The results showed that the prepared Cys@Au-Ag/AgCl nanocomposite exhibited high catalytic activity towards the reduction of toxic 4-NP to less toxic 4-AP within a few minutes using NaBH4 as a reducing agent. The catalytic reduction performance of Cys@Au-Ag/AgCl was optimized by studying the effect of various parameters on the catalytic reduction of 4-NP. Furthermore, the Cys@Au-Ag/AgCl nanocomposite was used for the catalytic reduction of  $K_3[Fe(CN)_6]$ 

in the presence of NaBH<sub>4</sub>. Additionally, the antibacterial activity of the nanocomposite was evaluated using disk diffusion method against some pathogenic Gram-positive and Gram-negative bacteria. The results showed that the Cys@Au-Ag/AgCl nanocomposite exhibited good antibacterial activity against drug-resistant clinical bacteria. Facile preparation, quick reduction time and antibacterial activity of Cys@Au-Ag/AgCl nanocomposite may open a new window to synthesize new nano-catalysts with enhanced properties for decontamination of organic and inorganic pollutants from water sources and reduce the spreading of diseases and infections in medical and industrial environments.

## Acknowledgements

The authors are grateful to the University of Guilan for financial support.

## **Compliance with Ethical Standards**

The authors declare that they have no conflict of interest. This article does not contain any studies involving animals or human participants performed by any of the authors.

# 4. References

- 1. M. J. Ndolomingo, N. Bingwa, R. Meijboom, *J. Mater. Sci.* **2020**, *55*, 6195–6241. **DOI**:10.1007/s10853-020-04415-x
- M. Azharuddin, G. H. Zhu, D. Das, E. Ozgur, L. Uzun, A. P. Turner, H. K. Patra, *Chem. Comm.* 2019, 55, 6964–6996.
  DOI:10.1039/C9CC01741K
- 3. T. H. Yang, J. Ahn, S. Shi, P. Wang, R. Gao, D. Qin, *Chem. Rev.* **2020**, *121*, 796–833. **DOI:**10.1021/acs.chemrev.0c00940
- 4. N. Gao, J. Xu, X. Li, G. Ling, P. Zhang, *Chem. Eng. J.* **2023**, 465, 142817–142831. **DOI:**10.1016/j.cej.2023.142817
- 5. I. Mustieles Marin, J. M. Asensio, B. Chaudret, ACS nano, **2021**, *15*, 3550–3556. **DOI:**10.1021/acsnano.0c09744
- M. S. Qatan, F. Arshad, M. Miskam, G. A. Naikoo, *Int. J. Environ. Sci. Technol.* 2024, 21, 5247–5268.
  DOI:10.1007/s13762-023-05429-z
- 7. K. Loza, M. Heggen, M. Epple, *Adv. Funct. Mater.* **2020**, 30, 1909260–1909273. **DOI:**10.1002/adfm.201909260
- J. Wang, C. An, M. Zhang, C. Qin, X. Ming, Q. Zhang, Can. J. Chem. 2012, 90, 858–864. DOI:10.1139/v2012-079
- P. C. Kuo, C. W. Lien, J. Y. Mao, B. Unnikrishnan, H. T. Chang, H. J. Lin, C. C. Huang, *Anal. Chim. Acta*, 2018, 1009, 89–97.
   DOI:10.1016/j.aca.2018.01.018
- K. Sapkota, S. S. Han, New J. Chem. 2017, 41, 5395–5402.
  DOI:10.1039/C7NJ00764G
- 11. N. R. Barveen, T. J. Wang, Y. H. Chang, *Chem. Eng. J.* **2021**, 423, 130191–130203. **DOI:**10.1016/j.cej.2021.130191
- T. B. Devi, M. Ahmaruzzaman, ChemistrySelect, 2017, 2, 5950–5957. DOI:10.1002/slct.201700601

- H. J. Ryu, H. L. Kim, J. H. Joo, J. S. Lee, Catal. 2020, 10, 405–408 DOI:10.3390/catal10040405
- J. Liu, Z. Wu, Q. He, Q. Tian, W. Wu, X. Xiao, C. Jiang, *Nanoscale Res. Lett.* **2019**, *14*, 1–13.
  DOI:10.1186/s11671-019-2862-9
- R. Nehru, T. W. Chen, S. M. Chen, T. W. Tseng, X. Liu, *Int. J. Electrochem. Sci.* 2018, 13, 7778–7788.
  DOI:10.20964/2018.08.14
- P. Sarkar, A. Dey, J. Environ. Chem. Eng. 2020, 8, 104347– 104355. DOI:10.1016/j.jece.2020.104347
- 17. T. K. Das, N. C. Das, *Int. Nano Lett.* **2022**, *12*, 223–242. **DOI:**10.1007/s40089-021-00362-w
- A. O. Cardoso Juarez, E. Ivan Ocampo Lopez, M. K. Kesarla,
  N. K. R. Bogireddy, ACS omega, 2024, 9, 33335–33350.
  DOI:10.1021/acsomega.4c04185
- K. S. Hayes, Appl. Catal. A: Gen. 2001, 221, 187–195.
  DOI:10.1016/S0926-860X(01)00813-4
- C. Zhang, R. Zhang, S. He, L. Li, X. Wang, M. Liu, W. Chen, *ChemCatChem.* 2017, 9, 980–986.
   DOI:10.1002/cctc.201601364
- Z. F. Jiang, F. M. Tian, K. M. Fang, Z. G. Wang, L. Zhang, J. J. Feng, A. J. Wang, J. Colloid. Interface Sci. 2025, 677, 718–728.
  DOI:10.1016/j.jcis.2024.08.027
- 22. M. J. Vaidya, S. M. Kulkarni, R. V. Chaudhari, *Org. Process Res. Dev.* **2003**, *7*, 202–208. **DOI:**10.1021/op025589w
- 23. N. Arora, A. Mehta, A. Mishra, S. Basu, *Appl. Clay Sci.* **2018**, *151*, 1–9. **DOI:**10.1016/j.clay.2017.10.015
- M. Rocha, C. Pereira, C. Freire, Colloids Surf. A: Physicochem. Eng. Asp. 2021, 621, 126614–126627.
   DOI:10.1016/j.colsurfa.2021.126614
- K. Hareesh, R. P. Joshi, D. V. Sunitha, V. N. Bhoraskar, S. D. Dhole, *Appl. Surf. Sci.* **2016**, *389*, 1050–1055.
  **DOI:**10.1016/j.apsusc.2016.08.034
- S. D. Oh, M. R. Kim, S. H. Choi, J. H. Chun, K. P. Lee, A. Gopalan, C. G. Hwang, K. Sang-Ho, O. J. Hoon, *J. Ind. Eng. Chem.* 2008, 14, 687–692. DOI:10.1016/j.jiec.2008.04.008
- S. Velpula, S. R. Beedu, K. Rupula, *Int. J. Biol. Macromol.* 2021, 190, 159–169. DOI:10.1016/j.ijbiomac.2021.08.211
- A. M. Mostafa, E. A. Mwafy, N. S. Awwad, H. A. Ibrahium, J. Mater. Sci.: Mater. Electron. 2021, 32, 11978–11988.
  DOI:10.1007/s10854-021-05827-4
- 29. S. Kumar, *EClinicalMedicine*, **2021**, *41*, 101221 **DOI:**10.1016/j.eclinm.2021.101221
- S. K. Ahmed, S. Hussein, K. Qurbani, R. H. Ibrahim, A. Fareeq, K. A. Mahmood, M. G. Mohamed, *J. Med. Surg. Public Health*, 2024, 2, 100081–100089.
  DOI:10.1016/j.glmedi.2024.100081
- 31. A. Brandelli, A. C. Ritter, F. F.Veras, Antimicrobial activities of metal nanoparticles. Metal nanoparticles in pharma, Springer, **2017**, pp.337–363.
  - **DOI:**10.1007/978-3-319-63790-7\_15
- K. Gold, B. Slay, M. Knackstedt, A. K. Gaharwar, Adv. Therap.
  2018, 1, 1700033–1700049.
  DOI:10.1002/adtp.201700033
- 33. A. Laganà, G. Visalli, F. Corpina, M. Ferlazzo, A. Di Pietro, A. Facciolà, *Eur. Rev. Med. Pharmacol. Sci.* **2023**, *27*, 3645–3663.

- C. Silvia Pop, D. Hussien, M. Popa, A. Mares, A. Mihai Grumezescu, R. Grigore, V. Lazar, M. Carmen Chifiriuc, M. Sakizlian, E. Bezirtzoglou, S. Bertesteanu, Curr. *Top. Med. Chem.* 2015, *15*, 1577–1582.
  - **DOI:**10.2174/1568026615666150414125015
- M. C. Sportelli, R. A. Picca, N. Cioffi: Nano-Antimicrobials Based on Metals. Novel antimicrobial agents and strategies: Wiley-VCH, Weinheim, Germany, 2014, pp. 181–218. DOI:10.1002/9783527676132.ch8
- S. Siddiqui, S. Shawuti, Sirajuddin, J. H. Niazi, A. Qureshi, Ind. Eng. Chem. Res. 2019, 58, 8035–8043.
   DOI:10.1021/acs.iecr.9b00016
- Z. Piri, Z. Moradi–Shoeili, A. Assoud, *Inorg. Chim. Acta*, 2019, 484, 338–346. DOI:10.1016/j.ica.2018.09.054
- S. Yallappa, J. Manjanna, B. L. Dhananjaya, Spectrochim. Acta-A: Mol. Biomol. Spectrosc. 2015, 137, 236–243.
  DOI:10.1016/j.saa.2014.08.030
- S. S. Godipurge, S. Yallappa, N. J. Biradar, J. S. Biradar, B. L. Dhananjaya, G. Hegde, K. Jagadish, G. Hegde, *Enzyme Microb. Technol.* 2016, 95, 174–184.
  DOI:10.1016/j.enzmictec.2016.08.006
- Y. H. Li, P. Tan, X. Q. Liu, D. D. Zu, C. L. Huang, L. B. Sun, J. Nanosci. Nanotechnol. 2015, 15, 4373–4379.
  DOI:10.1166/jnn.2015.9590
- 41. S. F. Parker, Chem. Phys. **2013**, *424*, 75–79. **DOI:**10.1016/j.chemphys.2013.04.020
- I. Feliciano-Ramos, M. Caban-Acevedo, M. A. Scibioh, C. R. Cabrera, *J. Electroanal. Chem.* 2010, 650, 98–104.
  DOI:10.1016/j.jelechem.2010.09.001
- 43. S. Diamai, D. P. Negi, Spectrochim. Acta-A: Mol. Biomol. Spectrosc. **2019**, 215, 203–208. **DOI**:10.1016/j.saa.2019.02.101

- 44. Z. Xu, H. Zhang, S. Liu, B. Zhang, H. Zhong, D. S. Su, *Int. J. Hydrogen Energy.* **2012**, *37*, 17978–17983. **DOI:**10.1016/j.ijhydene.2012.09.050
- R. Madhushree, J. R. J. UC, D. Pinheiro, S. D. KR, *Appl. Surf. Sci. Adv.* 2022, *10*, 100265–100273.
  DOI:10.1016/j.apsadv.2022.100265
- Y. Gao, J. Fang, Y. Zhang, C. Zhang, S. Zhao, Y. Zhou, M. Huang, X. Sheng, *Appl. Organomet. Chem.* 2018, 32, 4208–4219
- J. Fu, S. Wang, X. Wang, Y. Yan, K. Wang, M. Gao, Q. Xu, J. Porous Mater. 2017, 25, 1081–1089.
  DOI:10.1007/s10934-017-0519-6
- 48. Y. Yan, J. Fu, M. Wang, S. Liu, Q. Xin, Z. Chen, Q. Xu, RSC Advances, 2016, 6, 24921–24928. DOI:10.1039/C6RA02158A
- B. Duan, F. Liu, M. He, L. Zhang, Green Chemistry, 2014, 16, 2835–2845. DOI:10.1039/C3GC42637H
- Y. Chen, L. Feng, S. M. Sadeghzadeh, RSC advances, 2020, 10, 19553–19561. DOI:10.1039/D0RA01136C
- R. Aguilar-Garay, L. F. Lara-Ortiz, M. Campos-López, D. E. Gonzalez-Rodriguez, M. M. Gamboa-Lugo, J. A. Mendo-za-Pérez, Á. Anzueto-Ríos, D. E. Nicolás-Álvarez, *Pharmaceuticals*, 2024, 17, 1134. DOI:10.3390/ph17091134
- Y. Wang, J. Wan, R. J. Miron, Y. Zhao, Y. Zhang, Nanoscale,
  2016, 8, 11143–11152. DOI:10.1039/C6NR01114D
- Q. Li, F. Lu, H. Ye, K. Yu, B. Lu, R. Bao, Y. Xiao, F. Dai, G. Lan, ACS Sustain. Chem. Eng. 2018, 6, 9813–9821.
   DOI:10.1021/acssuschemeng.8b00931
- S. Wang, Y. Wang, Y. Peng, X. Yang, ACS appl. Mater. Interfaces, 2019, 11, 8461–8469. DOI:10.1021/acsami.8b22143
- X. Hu, X. Xu, F. Fu, B. Yang, J. Zhang, Y. Zhang, S. S. B. Touhid, L. Liu, Y. Dong, X. Liu, J. Yao, *Carbohydr. Polym.* 2020, 248, 116777. DOI:10.1016/j.carbpol.2020.116777

## **Povzetek**

V tej raziskavi smo s preprosto hidrotermalno metodo pripravili strukturo nanoklastrov na osnovi zlata in srebra, modificiranih z L-cisteinom (Cys@Au-Ag/AgCl). Cys@Au-Ag/AgCl je pokazal učinkovito katalitsko aktivnost pri hitri redukciji 4-nitrofenola (4-NP) v manj toksičen 4-aminofenol (4-AP) ob prisotnosti NaBH4 kot reducenta, pri čemer je bila reakcija zaključena v nekaj minutah s hitrostno konstanto  $6.1 \times 10^{-3} \text{ s}^{-1}$ . Katalitsko učinkovitost Cys@Au-Ag/AgCl smo optimirali s preučevanjem vpliva različnih parametrov na katalitsko redukcijo. Poleg tega smo nanokompozit Cys@Au-Ag/AgCl uporabili tudi za katalitsko redukcijo  $K_3[Fe(CN)_6]$  v prisotnosti NaBH4, pri čemer je bila izmerjena konstanta reakcijske hitrosti  $1.73 \times 10^{-2} \text{ s}^{-1}$ . Ocenili smo tudi protibakterijsko aktivnost nanokompozita Cys@Au-Ag/AgCl proti pogostim na zdravila odpornim gram-pozitivnim bakterijam (Bacillus subtilis in Staphylococcus aureus) ter gram-negativnim bakterijam (Pseudomonas aeruginosa in Escherichia coli). Rezultati so pokazali, da multifunkcionalni nanokompozit Cys@Au-Ag/AgCl izkazuje dobro protibakterijsko delovanje proti tem klinično pomembnim odpornim bakterijam.



Except when otherwise noted, articles in this journal are published under the terms and conditions of the Creative Commons Attribution 4.0 International License